Chapter 8
Photo-Switching of Circularly Polarized Luminescence

Takuya Nakashima and Tsuyoshi Kawai

Abstract Circularly polarized luminescence (CPL) emission from chiral molecular systems is readily switched by means of external stimuli such as temperature, solvent, chemicals, and light irradiation. Since CPL is one of the emission phenomena, it can be modulated in a similar manner to the emission switching. The ON-OFF switching of emission intensity of chiral molecular systems may simply lead to the modulation of CPL intensity. Apart from the modulation of emission intensity, the chiral structures including chiral arrangement of fluorophores or metal coordination geometries are switched by external stimuli, changing the dissymmetry factors, i.e., the quality of CPL. In this chapter, we review the design of chiroptical photo-switches based on photochromic molecules that modulate the CPL property in response to photo-irradiation in a dynamic manner.

8.1 Introduction

The CPL technique is expected to find potential applications in sensors, display, and advanced information technologies including anti-counterfeiting labeling. Recent research has made efforts in the manipulation and modulation of CPL activity to further develop these technologies including supramolecular approaches [1–11]. High-speed switching of CPL in a dynamic manner by external stimuli should be of particular interest for the application in cryptographic communication as a technology for information security [12–14]. Light is one of the external inputs for various practical applications, whereby one can control the physico-chemical properties of active materials with precise spatiotemporal control in a remote and noninvasive manner. In this context, chiroptical photo-switches are promising materials for the dynamic modulation of CPL property with imparting luminescent capability to photo-responsive molecules [15]. Photo-switching of luminescent

T. Nakashima (✉) · T. Kawai (✉)
Division of Materials Science, Graduate School of Science and Technology, Nara Institute of Science and Technology, Ikoma, Nara, Japan
e-mail: ntaku@ms.naist.jp; tkawai@ms.naist.jp

T. Mori (ed.), *Circularly Polarized Luminescence of Isolated Small Organic Molecules*, https://doi.org/10.1007/978-981-15-2309-0_8

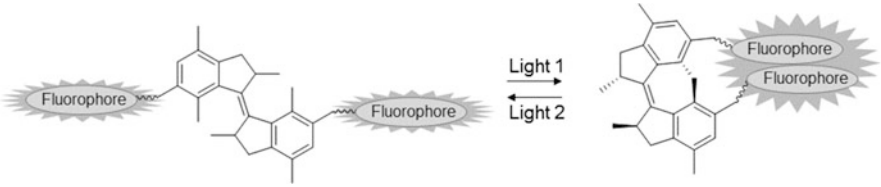

Fig. 8.1 Change of the intramolecular interaction between fluorophores in response to the geometrical change of photochromic molecule

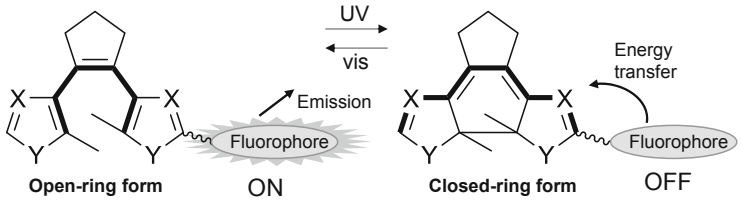

Fig. 8.2 ON-OFF emission switching based on a change in the electronic structure of photochromic diarylethene

property has been demonstrated by exploiting changes in the electronic and geometric structures of photochromic molecules [16–18]. For example, *trans-cis* photoisomerization of thioindigo [19] and overcrowded alkene [20] readily controlled the arrangement of two fluorophore units in an intramolecular manner, modulating their emission between the monomeric and dimeric (excimer) ones (Fig. 8.1). The photoinduced electrocylization reaction in diarylethenes [17] and fulgido [21] from the open-ring to the closed-ring form induces a dramatic red-shift of absorption band from UV to the visible region. This change in the electronic structure often quenches the emission of fluorophores attached to the photochromic unit based on the energy transfer with an appreciable spectral overlap between the emission band of fluorophores and the absorption band corresponding to the closed-ring form of photochromes (Fig. 8.2). Since most of photochromic reactions, especially the 6π-based electro-cyclization reactions, proceed in a stereospecific manner with high quantum efficiency, the incorporation of photochromic units in a chiral fluorescent molecule is an effective way to control the chiroptical property including CPL emission of molecular system by means of light irradiation.

8.2 Quenching of CPL from Chiral π-Conjugated Polymers by Photochromic Reaction of Diarylethene

The first example of ON-OFF photo-switching of CPL was demonstrated by Akagi and coworkers [22]. Conjugated polymers based on poly(*p*-phenylene) and poly (bithenylene-phenylene) are linked with a photo-responsive diarylethene moiety

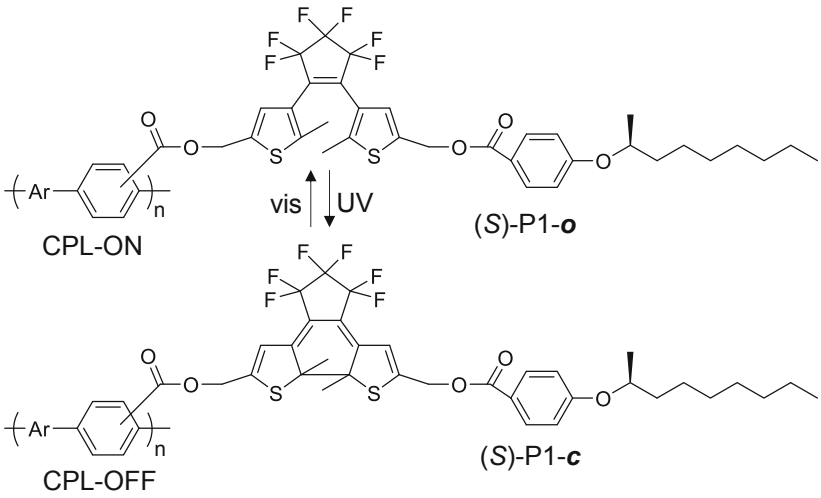

Fig. 8.3 Structure and photoreaction of photo-responsive chiral conjugated polymer **P1**

tethering a chiral alkyl chain as a side-chain unit (**P1**, Fig. 8.3). The conjugated polymers exhibited an optical activity in the cast films with circular dichroism (CD) and CPL activities corresponding to the π-π∗ transition in the π-conjugated main chain. The cast films afforded a bisignate split CD profile in the π-π∗ transition region of the main chain, suggesting a one-handed helical inter-chain π-stacking structure based on the exciton coupling theory [23]. Although the chiral alkyl chain unit was introduced in the side chain through the photochromic moiety, the chirality information was transferred to the inter-polymer main-chain interactions, displaying the CPL activity in the film state in a similar manner to other conjugated polymers modified with chiral side-chain units [24–27]. The photochromic unit in the conjugated polymers **P1**-***o*** maintained the photo-responsiveness in the cast films. The fluorescence and CPL of the π-conjugated main chain were readily quenched by means of UV irradiation through energy transfer from the main chain to the photogenerated closed-ring moiety of diarylethene in the side chain. The CPL activity was recovered by the cyclo-reversion reaction of the diarylethene moiety upon visible light irradiation and the ON-OFF photo-switching behavior was repeated over 10 cycles.

8.3 Photo-Switching of CPL Based on Pyrene-Bearing Photo-Responsive Foldamer

The inter-chromophoric interactions usually provide the most significant contributions to the chiroptical property in molecular systems as explained by the exciton coupling theory [23, 28]. As a rough framework of the theory, the chiral arrangement

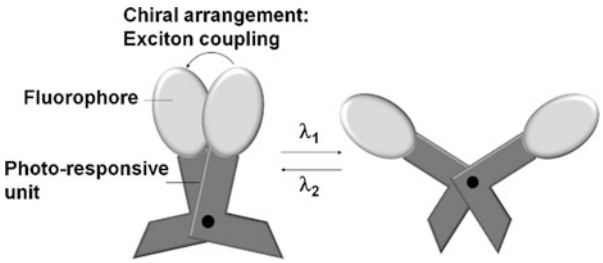

Fig. 8.4 Schematic design of a CPL-photo-switch

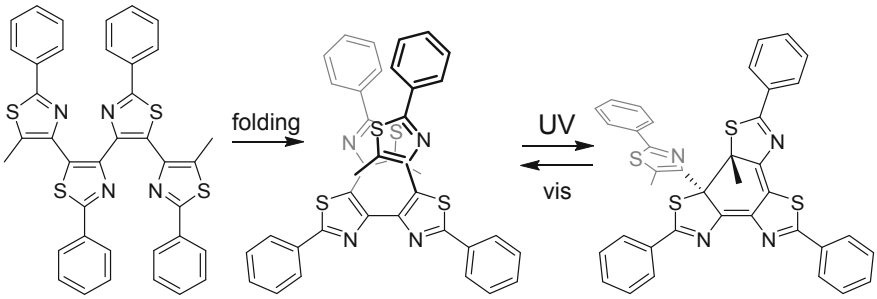

Fig. 8.5 Conformational folding and photoreactions of tetra(2-phenylthiazole)

of multiple chromophores (or fluorophores) could be an important source of optical chirality including CD and CPL activities. On the basis of the theory, the chiroptical switch can be achieved if the external stimuli modulate the chiral chromophoric arrangement in molecular systems. Figure 8.4 depicts a schematic design of possible CPL-photo-switch. The photo-responsive unit with a chirally controlled geometry should carry multiple fluorophores, arranging them in a chiral manner so that the exciton coupling interaction operates on them. The photo-irradiation induces the structural change in the photo-responsive unit, leading to a change in the fluorophoric arrangement to modulate the inter-fluorophore exciton coupling.

Chiral photochromic scaffold with a helical secondary structure was employed as a platform for modulating CPL activity through a control of chiral fluorophore arrangement in an intramolecular manner. The central ethene part of diarylethene was replaced with a heteroaromatic ring to form a tetra-arylene scaffold with keeping the photochromic capability [29]. The use of oligo-heteroarylene framework enables the molecule to take advantage of inter-heteroaryl-unit interactions involving heteroatoms so that they can adopt the molecular conformation suitable for the electrocyclization reaction [30–33]. The extension of heteroaromatic units led to the formation of helical foldamers with photo-reactivity [34–36]. Tetra-arylenes composed of 2-phenylthiazole unit with a cis-cisoid-like connectivity form a one-turn helical secondary structure as the most stable conformation, which is also suitable for the stereo-specific electro-cyclization reaction (Fig. 8.5) [34–36]. The incorporation of chiral groups as a side-chain unit readily controlled the handedness of helicity. For the design of CPL photo-switch, a pyrene group was introduced at each

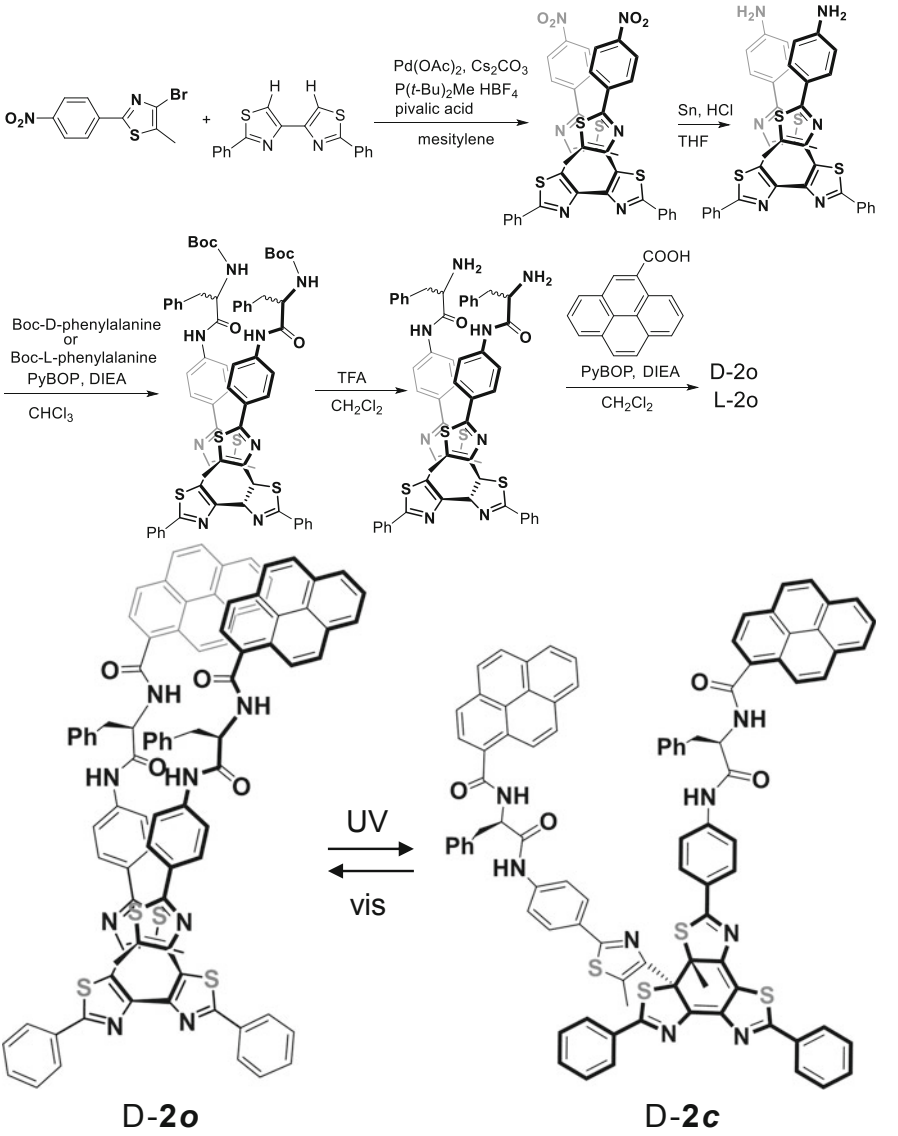

Fig. 8.6 Synthetic scheme and photochromic reaction of pyrene-modified tetrathiazole **2**

end of tetra(2-phenylthiazole) through a chiral phenylalanine spacer (D- or L-**2*o***, Fig. 8.6) [37]. The chiral spacer controls the handedness of a helix, arranging two pyrene units in a chiral manner. The photochromism in the tetrathiazole unit gives rise to a large structural change to form a ring-closed photoisomer **2*c***, changing the position and orientation of two pyrene units.

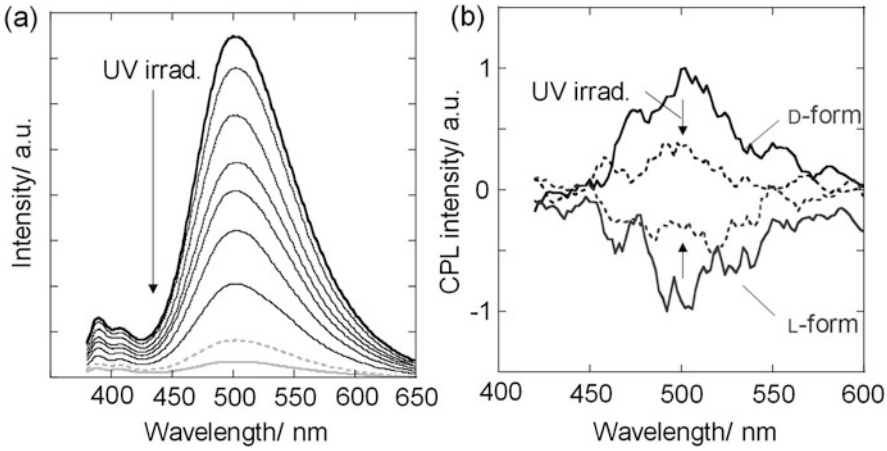

Fig. 8.7 (**a**) Fluorescence and (**b**) CPL spectral change of **2*o*** upon UV (365 nm) irradiation in chloroform. Traces in (**a**) were measured with an irradiation interval of 5 s. Dashed line plots in (**b**) correspond to CPL spectra at the photostationary state (PSS) under UV irradiation

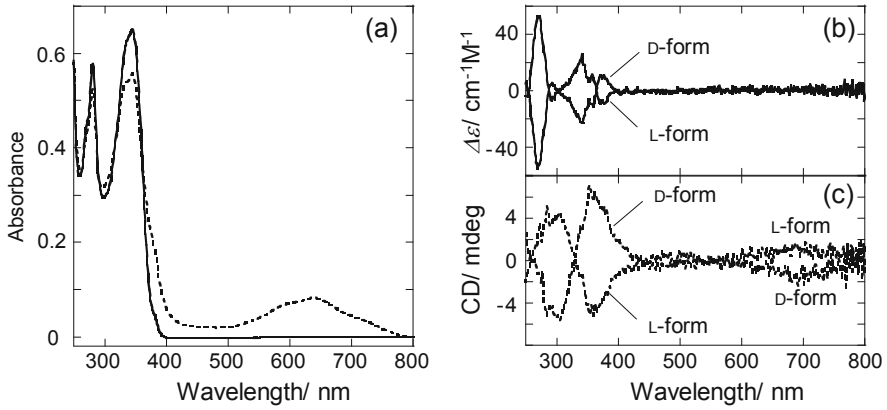

Fig. 8.8 Absorption (**a**) and CD (**b**, **c**) spectral change of **2** in chloroform (8.7×10^{-6} M) upon UV irradiation. (**a**) Solid line, L-**2*o***; dashed line, at photo-stationary state (PSS). (**b**, **c**) Solid lines, **2*o***; dashed lines, at PSS

The conformational behavior of **2*o*** in solution was characterized by means of ^{1}H NMR, CD, fluorescence, and CPL measurements. The ^{1}H NMR study suggested the operation of intramolecular interactions including hydrogen bonding between the amide groups and π-π stacking between the pyrene units. Together with this result, the strong excimer-like emission observed at 500 nm and the suppressed monomer emission band at 390 nm (Fig. 8.7a) clearly support the preferential adoption of a compactly folded conformation as depicted in Fig. 8.6. The CD measurement confirms the chirality induction in the secondary structure of the main framework in **2*o*** (Fig. 8.8b). The positive- and negative-first Cotton effect signals for D- and

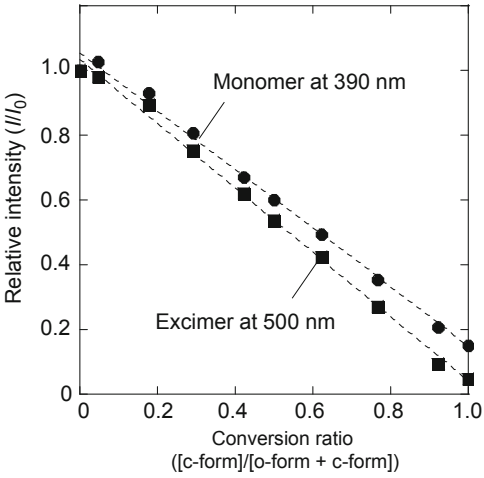

Fig. 8.9 Plots of relative emission intensity in monomer (circle, at 390 nm) and excimer (square, at 500 nm) emission. I_0 corresponds to the intensity at a conversion of 0

L-***2o***, respectively, suggest the preferential formation of right- and left-handed helices, respectively. In the helical molecular geometry of ***2o***, the pyrene units were stacked in a chiral manner. Owing to this chiral arrangement, compounds ***2o*** are CPL active showing a positive and negative CPL signal in the region of excimer-like emission band for D- and L-isomers, respectively (Fig. 8.7b). The signs of CPL signal coincide with those of the first Cotton effect observed in the CD study. The anisotropy factor, which is given by the equation $g_{\mathrm{lum}} = 2(I_{\mathrm{L}} - I_{\mathrm{R}})/(I_{\mathrm{L}} + I_{\mathrm{R}})$, where I_{L} and I_{R} are the intensities of the left- and right-handed circularly polarized emission, respectively, was estimated to be 0.01. This relatively high value for the small chiral organic molecule [38] is consistent with previously reported values for chiral pyrene excimers [39, 40].

UV irradiation to ***2o*** solution resulted in the emergence of an absorption band in the visible region extended to 800 nm due to the formation of ***2c*** (Fig. 8.8a). Meanwhile, a drastic change was recorded in the CD spectra, in which broad CD signals at the wavelength of the visible absorption band of photo-products emerged (Fig. 8.8c). The emergence of CD band in the visible region suggested the diastereo-selective photoreaction in the 6π-system. A combination of ^{1}H NMR and chiral HPLC studies for the photo-products indicated an absolute stereo-selective ring-cyclization reaction for **2**. The intensity of both monomer and excimer-like emission bands decreased with the progress of ring-cyclization reaction by the UV irradiation (Fig. 8.7a). Along with the decrease in the excimer-like emission intensity by the photo-isomerization, the CPL intensity decreased (Fig. 8.7b). Since the CPL measurement was performed at a relatively high concentration (1.7×10^{-4} M) in comparison to that for absorption spectra, the conversion ratio was not enough to achieve the completely off-state (Fig. 8.7b). In principle, the isolated ***2c*** gave a negligible emission quantum yield far less than 0.1%.

The emission from both the monomer and the excimer decreased in a liner fashion as a function of the conversion ratio to the colored form ***2c*** (Fig. 8.9). The quenching

of monomer emission should be attributed to an energy transfer mechanism by the increased absorbance in the range of 380–410 nm in ***2c***, which well overlaps with the pyrene monomer emission (Figs. 8.7a and 8.8a). The same mechanism partly explains the quenching of the excimer-like emission at 500 nm. Although the spectral overlap of excimer-like band at around 500 nm with absorption in ***2c*** is not as prominent as that of monomer emission band, the quenching of excimer-like emission was a little more significant than that of monomer emission (Fig. 8.9). This result might be attributed to the appreciable contribution of geometrical change in ***2c*** as depicted in Fig. 8.4. The structural change in the arrangement of pyrene units was supported by an upfield shift of amide-protons from ***2o*** to ***2c*** in the ^{1}H NMR study, corresponding to the dissociation of intramolecular hydrogen bonding interactions.

8.4 Dynamic Switching of Hierarchical Chirality in Photo-Responsive Dinuclear Complexes

Unlike most chiral organic fluorophores affording CPL activity with a limited $|g_{lum}|$ value less than 0.05, large $|g_{lum}|$ values over 0.1 have been reported for the magnetic dipole transition in europium(III) complexes [41–45]. Eu(III) complexes have also been combined with 6π-based photochromic units to modulate the photoluminescence intensity [46–48]. Photochromic reaction is expected to modulate the emission property of Eu(III) ion through electronic and geometrical changes in the photochromic ligand. For the purpose of induction and modulation of chirality in the Eu(III) coordination cores, the pyrene unit in ***2o*** was replaced with a coordinating ligand [49]. Terpyridine (**terpy**) ligands were introduced at both ends of the helical tetrathiazole scaffold, forming ***3o*** with Eu(III) ions and β-diketonato ligands (**tta**) (Fig. 8.10). The local coordination site **Eu(terpy)(tta)$_3$** including asymmetric **tta** ligands is considered to have intrinsic chirality with eight possible chiral nine-coordination structures. The incorporation of **Eu(terpy)(tta)$_3$** sites in the chiral helical structure is expected to bring the complex sites close together in a chiral arrangement. This chiral arrangement should serve as a chiral perturbation to the coordination sites and one specific chiral coordination structure is preferentially formed among the eight possible ligand orientations, inducing optical activity in ***3o***. Thus the point chirality in the amino acid spacer is expected to be transferred over hierarchy. The point chirality in the amino acid spacer was first introduced as a primary structure of a foldamer **3**, controlling the handedness in the helical conformation as a secondary structure. The handedness-controlled chiral helical conformation of **3** arranges the inherently chiral coordination cores in a chiral manner, inducing the biased formation of one-handed chiral ligand orientation in the coordination sites.

3o exhibited bright red emission from Eu(III)-centered f-f transitions with an apparent emission quantum yield (Φ_{lum}) of 0.20 ($\lambda_{ex} = 360$ nm) and an emission lifetime of 0.55 ms in $CDCl_3$. The photoluminescence spectrum (Fig. 8.11a) gave

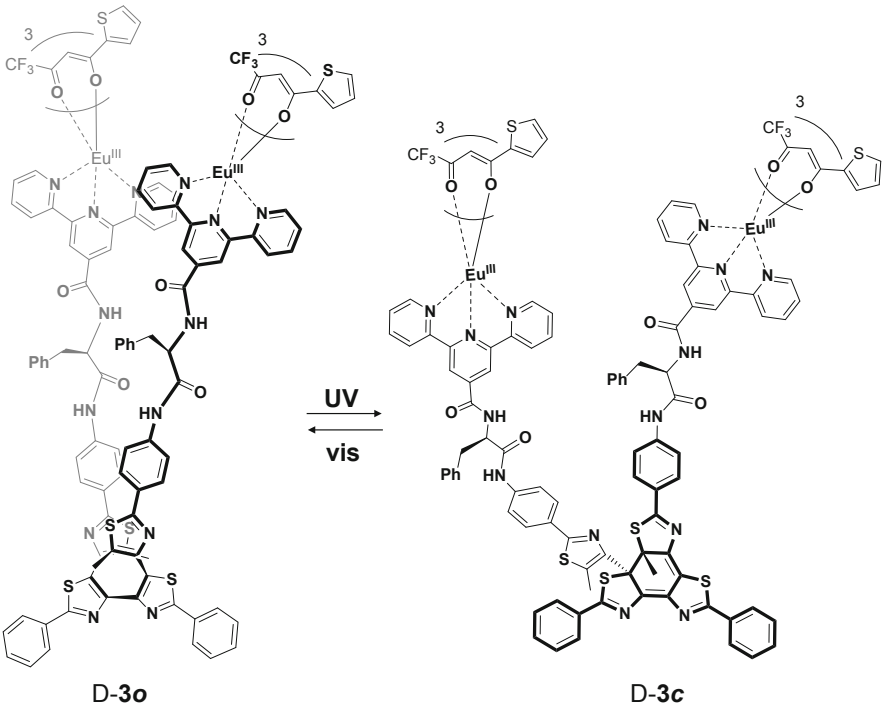

Fig. 8.10 Photo-switching reaction of D-**3**

emission peaks at 580 ($^5D_0 \rightarrow {}^7F_0$), 595 ($^5D_0 \rightarrow {}^7F_1$), and 620 nm ($^5D_0 \rightarrow {}^7F_2$). Meanwhile, mirror-image CPL signals were obtained for the enantiomer pair of ***3o*** complexes at the bands of $^5D_0 \rightarrow {}^7F_1$ and $^5D_0 \rightarrow {}^7F_2$ transitions corresponding to magnetic and electronic dipole ones, respectively (Fig. 8.11b). The emergence of CPL signals clearly suggested the induction of optical activity in the dinuclear Eu (III) complexes. We obtained $|g_{lum}|$ values of 0.1 at the magnetic-dipole transition band, which are ten times larger than that of the pyrene-containing ***2o***. The enantiomeric enrichment in the Eu(III)-complex sites was further confirmed with the induction of CD signal in the f-f transition absorption bands by replacing Eu(III) ions with Nd(III) ions (***3o*(Nd)**). The mirror-image CD spectra over 500 nm corresponding to the f-f transition region in Nd(III) ion clearly support that the chirality is indeed induced as a coordination chirality in the local Ln(III) complex sites.

To further discuss the origin of optical activity, **tta** ligand in ***3o*** were replaced with a number of β-diketonato ligands both with symmetric and asymmetric structures. The Eu(III) complexes with asymmetric β-diketonato ligands having a trifluoromethyl (CF_3) and aromatic units showed much better photoluminescence and CPL efficiency compared with those with symmetric β-diketonato ligands. This result further confirms that the enriched population of an enantiomeric coordination

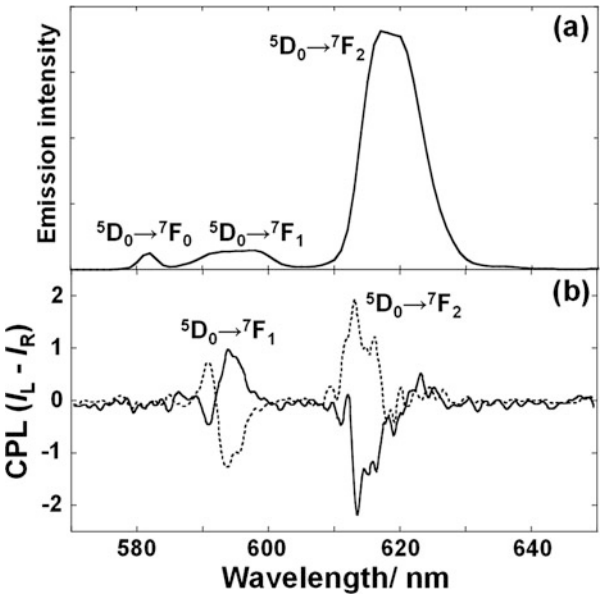

Fig. 8.11 (**a**) Photoluminescence and (**b**) CPL spectra of D-(solid lines) and L-**3*o*** (dashed lines) in $CHCl_3$

structure in terms of chiral ligand orientation was the primary source as the origin of chirality induction in **3*o***.

UV irradiation to a chloroform solution of **3*o*** resulted in the emergence of an absorption band in the visible region due to the formation of closed-ring isomer in the photochromic framework in a similar manner to **2**. The photo-reaction also induced a decrease in the emission intensity in the whole spectral region, and the Φ_{lum} value dropped to 0.03 at the PSS with a conversion ratio of 85% (Fig. 8.12a). The decrease in the emission intensity and lifetime were attributed to the Förster resonance energy transfer (FRET) mechanism from the excited state of Eu(III) to the photochromic center [46–48]. The photo-cyclization reaction of the photochromic backbone of **3** also promoted a decrease in CPL intensity (Fig. 8.12b). Given that the enantiomeric structure induced in the Eu(III) complex sites is maintained after the photoreaction, the g_{lum} value should be unchanged even if the CPL intensity decreases. However, the $|g_{lum}|$ value decreased to <0.01, affording a large modulation amplitude in CPL dissymmetry, $|\Delta g_{lum}| > 0.09$. The decrease in the dissymmetry factor should be attributed to the cancellation in the enrichment of one-hand chiral coordination structure in the Eu(III) complex sites with the aid of labile coordination character [50].

Meanwhile, UV irradiation to **3*o*(Nd)** gave rise to an emergence of a broad absorption band in the visible band which is superimposed with the $4I_{9/2} \rightarrow 4G_{5/2}$ transition at 580 nm in Nd(III) ion (Fig. 8.12c). This spectral change accompanies the gradual progression of broad negative and positive CD signals over 500 nm for D- and L-**3(Nd)**, respectively, supporting the diastereo-selective formation of the closed-ring isomer (***c***-forms). The positive and negative CD signals corresponding to $4I_{9/2} \rightarrow 4G_{5/2}$ transition band at 580 nm observed for D- and L-**3*o*(Nd)**, respectively,

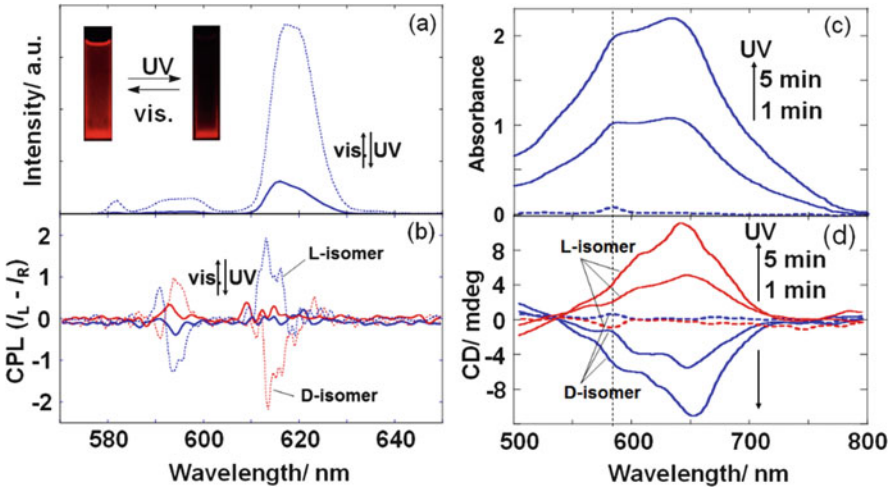

Fig. 8.12 (**a**) Photoluminescence and (**b**) CPL spectral change of **3** in $CHCl_3$ before (broken lines) and after photo-irradiation to achieve PSS under irradiation at 365 nm (solid lines). (**c**) Absorption and (**d**) CD spectral change of **3(Nd)** before (broken lines) and after UV irradiation (solid lines) for 1 and 5 min in $CHCl_3$

remained in the CD spectra after 1 min of irradiation (Fig. 8.12d). The apparent features of these positive and negative signals at 580 nm diminished as the photo-reaction proceeded after 5 min of irradiation while the sharp absorption bump was still apparent in the absorption profile (Fig. 8.12c). This result suggests that the preferential formation of enantiomeric coordination structure in the Ln(III)-complex sites was effective only in the helical structure, wherein the close contact between the complex sites is operative. The photo-induced helical to non-helical transformation of the main framework switches off the close arrangement of the coordination units. The labile coordination character of lanthanide ions should negate the enrichment of enantiomeric coordination structure, diminishing the optical activity (Fig. 8.13).

8.5 Photo-Switching of CPL in Photo-Responsive Molecular Self-Assemblies

Chiroptical properties have often been demonstrated to enhance in chiral supramolecular assemblies as supramolecular chirality [51, 52]. The CPL property was highly dependent on the supramolecular morphologies, wherein the ordering of building unit varies [4, 5]. Photo-responsive azobenzene units were incorporated in a building block of a chiral supramolecular assembly (**4**; Fig. 8.14) [53]. (*S*)-(*E*, *E*)-**4** formed entangled helical fibers with a right-handed twist as a self-assembling structure, exhibiting an intense positive CD signal at 464 nm. (*R*)-**4** gave a similar morphology in the self-assembling state but with opposite twist and CD signal to

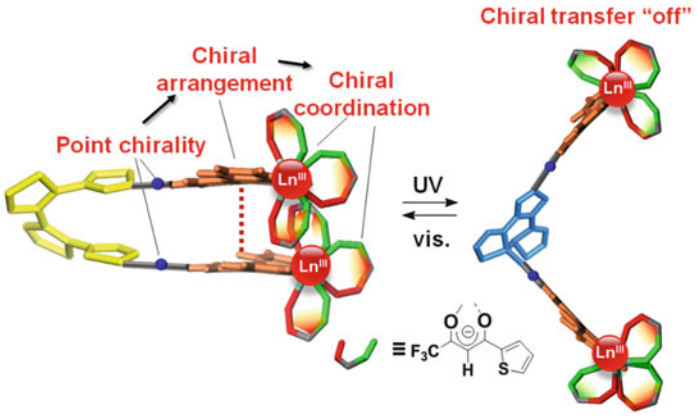

Fig. 8.13 Schematic illustration of hierarchical chirality transfer and its reversible modulation in the photo-responsive chiral dinuclear complex

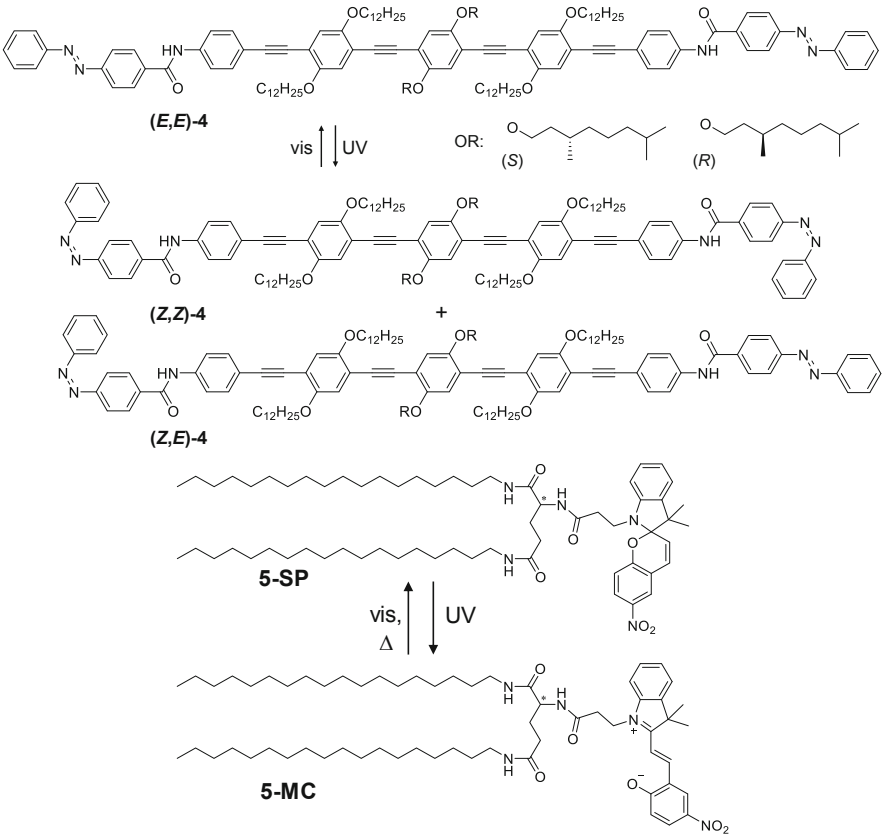

Fig. 8.14 Structures and photoreactions of photo-responsive chiral self-assembling molecules

(*S*)-**4**. Thus the chirality in the alkyl side chains was transferred as a helical molecular arrangement in the self-assemblies, affording an emergence of supramolecular chirality. Owing to the supramolecular chirality, the self-assembly of (*S*)-(*E*, *E*)-**4** gave a positive CPL signal with the g_{lum} value of 0.008. Although the photo-reaction of azobenzene moiety could not be induced in the self-assembling state, the dissociation of self-assembly with heating could enable the *E*-to-*Z* photo-isomerization. The photo-irradiated solution was cooled below 300 K and the inversion of CD signal sign was induced, thus reversing the supramolecular chirality. Along with the supramolecular chirality inversion, the CPL signal became negative with the g_{lum} value of -0.002. After the photo-irradiation, the supramolecular helicity in the fibrous assembly was also reversed. Photo-reactive spiropyran moiety was also introduced in a self-assembling chiral glutamate organogelator **5** (Fig. 8.14) [54]. **5-SP** formed helical nanofibers to gelatinize organic solvents, while fluorescent property was absent. Upon UV irradiation, the colorless organogel of **5-SP** turned blue with the formation of a merocyanine form (**5-MC**) with changing the micro-structures. **5-MC** exhibited red-color fluorescence, switching on the CPL activity. Alternate UV and visible light irradiations reversibly switched the CPL activity of organogel of **5** between ON and OFF states, respectively. A similar chiral glutamate compound having a photo-reactive cinnamic acid moiety was also demonstrated to reverse CPL sign in response to photo-dimerization reaction [55].

The photo-isomerization of azobenzene unit involves the rotational motion around the N–N bond in the excited state, which may prohibit the *trans*-to-*cis* isomerization in the self-assembling state of (*E*,*E*)-**4**. Therefore, dynamic in situ photo-switching of CPL activity in a supramolecular system had still remained a challenge. In comparison to the photo-reaction of azobenzene, the photo-cyclization reaction of 6π-system requires a smaller structural change, affording very efficient solid-state reactivity [17]. The CPL photo-switching molecules D- and L-***2o*** were employed as a building unit of self-assembly [56]. The emission turn-off behavior is expected to be amplified in such aggregation systems because the energy transfer based emission quenching operates not only in intramolecular but also in intermolecular manners [57, 58]. Compound ***2o*** was molecularly dispersed in chloroform, while it gave dispersion of nanoparticle assemblies in a mixture of chloroform/methylcyclohexane(MCH) (1:9 or 1:99) solvents. The transmission electron microscopy (TEM) observation revealed the formation of nanoparticle aggregates with an average diameter of ca. 250 nm in the chloroform/MCH (1:9) mixture at a concentration of 1.0×10^{-4} M (Fig. 8.15a). CD spectra exhibited mirror-image profiles in response to the stereochemistry in the amino-acid spacer with the same sign of first Cotton effect regardless of the solvent composition (Fig. 8.15b). The peak splitting patterns of MCH-rich solutions differ from those in molecularly dispersed chloroform solutions, suggesting the difference in the exciton coupling mode. The CD spectra for the MCH-rich solution should include intermolecular exciton coupling effect in the aggregates. The molar CD ($\Delta\varepsilon$), which is the parameter of CD amplitude, exhibited a pronounced increase in the MCH-rich solution compared to that in molecularly dispersed state.

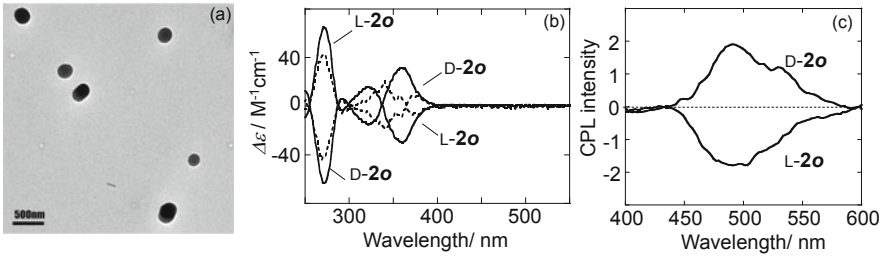

Fig. 8.15 (**a**) TEM image of aggregates formed by D-**2*o*** in chloroform/MCH (1:9) mixture solvent. (**b**) CD spectra of 2o in chloroform (broken lines) and chloroform/MCH (1:9) mixture solvent (solid lines). (**c**) CPL spectra of ***2o*** in chloroform/MCH (1:9) mixture solvent (concentration: 1.0×10^{-4} M)

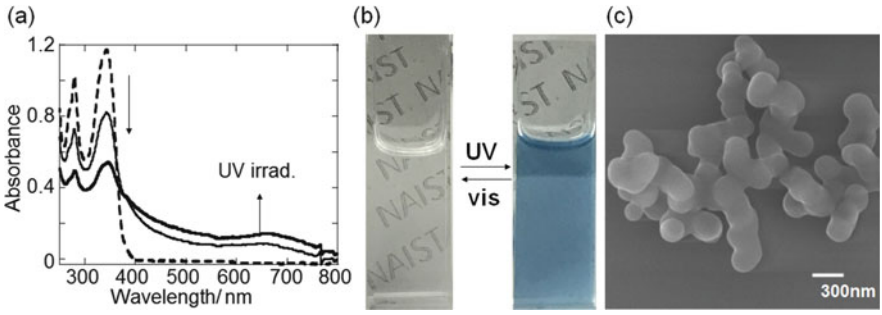

Fig. 8.16 (**a**) Absorption spectral change and (**b**) picture of photochromic reaction of D-**2*o*** upon UV irradiation in chloroform/MCH (1:9) (1.0×10^{-4} M). (**c**) SEM image of aggregates formed at the PSS of D-**2** in chloroform/MCH (1:9) (1.0×10^{-4} M)

The nanoparticle aggregates afforded appreciable CPL signals at 490 nm, which showed a shift to shorter wavelength in comparison to that in chloroform due to the less stabilization of excimer-like state in the less polar MCH-rich solvent (Fig. 8.15c). The dissymmetry factor $|g_{lum}|$ was a little enhanced to be 0.017 compared to that in molecularly dispersed state of 0.01, showing a good agreement with the enhanced $\Delta\varepsilon$ value observed in the CD measurement.

UV irradiation at 365 nm to the MCH-rich solution of ***2o*** induced the photoisomerization with the emergence of an absorption band at 650 nm corresponding to the formation of colored isomer ***2c*** (Fig. 8.16a). Interestingly, upon UV irradiation, the MCH-rich solution turned turbid at room temperature, suggesting the photoinduced secondary aggregation of nanoparticles (Fig. 8.16b). The clouding behavior was apparent in the absorption spectral change as an increase of background scattering (Fig. 8.16a). The colored isomer ***2c*** has a more rigid structure with an additional covalent bond compared to ***2o*** with a flexible conformation, leading to a decrease in the solubility of compound in MCH-rich solutions. In comparison to the increase in the absorption band in the visible region, the decrease of the absorption in the UV region was more prominent. This significant decrease should be attributed to

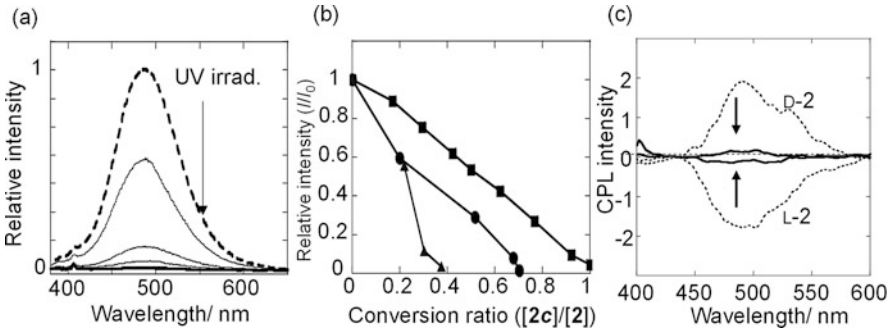

Fig. 8.17 (**a**) Emission spectral change of D-***2o*** upon UV irradiation in chloroform/MCH (1:99) solution (1.0×10^{-4} M). Before UV irradiation, broken line; at PSS achieved by the excitation at 365 nm, thick black line. (**b**) Plots of relative emission intensity as a function of a conversion ratio between D-***2o*** and **2c**. Square, in chloroform; circle, in chloroform/MCH (1:9); triangle, in chloroform/MCH (1:99) (concentration: 1.0×10^{-5} M). (**c**) CPL spectral change of D- and L-**2** before (broken lines) and after the UV irradiation at the PSS (solid lines) in chloroform/MCH (1:9) (concentration: 1.0×10^{-5} M)

the decrease of the solution concentration upon the secondary aggregation accompanied by the photo-cyclization reaction of **2**. The visible light irradiation above 440 nm bleach the solution color and the visible absorption band disappeared reversibly to give an absorption spectrum identical to that of ***2o*** with transparency in the visible range, indicating the dissolution of secondary aggregates.

SEM observation after the UV light irradiation clearly demonstrated the formation of secondary aggregates together with an increase in the size of nanoparticles (Fig. 8.16c). The photo-reaction seems to take place for the molecules on the surface of nanoparticles in the early stage of photo-conversion. The less solubility of the colored isomer ***2c*** in the MCH-rich solvent could reduce the colloidal stability of nanoparticles, leading to the further aggregation and fusion of nanoparticles. Intermolecular hydrogen bonding interactions are also possible in the colored form ***2c***, which may also drive the inter-nanoparticle aggregation.

The photoreaction also induced a decrease in the emission intensity in the whole spectral range (Fig. 8.17a). In the chloroform solution, the emission intensity decreased linearly as a function of conversion ratio (Fig. 8.17b). The more dramatic decrease in the emission intensity was observed in the MCH-rich solutions in comparison to that in the molecularly dispersed chloroform solution. The emission was almost completely quenched in the small conversion ratio values of 70 and 39% in chloroform/MCH (1:9) and (1:99) solvents, respectively (Fig. 8.17b). In a similar manner to the molecularly dispersed state in chloroform, the emission quenching is due to the FRET process from the excited state of pyrene moiety to the photochrome ring-closed part in ***2c***. The energy transfer process also take place in an intermolecular manner in the aggregates, enhancing the emission quenching efficiency in MCH-rich solvents. The FRET process from the pyrene moiety in the open-ring state ***2o*** to the ring-closed photochromic part in ***2c*** can apparently

contribute to the emission quenching [57, 58]. Furthermore, the secondary aggregation might also increase the probability of intermolecular energy transfer.

The reversible modulation of CPL intensity upon photo-irradiations was performed (Fig. 8.17c). Along with the emission quenching, the CPL signal also diminished. As demonstrated in the emission quenching study, the CPL signal intensity basically responds to the conversion ratio between **2*o*** and **2*c*** in a linear fashion in chloroform. However, the appreciable emission quenching did not need a high conversion ratio in the aggregate state (Fig. 8.17b), proposing the more efficient and high-contrast CPL photo-switching system. The CPL intensity ($I_L - I_R$) was reversibly switched between ON and OFF states for 8 cycles with consecutive UV-visible light irradiations.

8.6 Summary and Outlook

In this chapter, we introduced a design concept and several examples of CPL photoswitches which modulate CPL activity in response to light irradiation. Photoresponsive units are combined with fluorophore units in a chiral molecular system. The CPL intensity can be controlled by means of energy transfer quenching by the formation of a quencher unit upon photochromic reaction. The CPL activity is also controlled in terms of the exciton coupling modulation in response to the chiral geometrical change induced by the stereo-specific photo-reaction. The photoswitching effect could be enhanced in the chiral supramolecular systems.

Highly pure CPL could be generated by the use of selective reflection in a cholesteric liquid crystalline phase [59, 60]. Helical pitch, handedness, and arrangement of mesogens in such chiral liquid crystalline system can be modulated by the photo-reaction of chiral photochromic dopants [61–64]. High speed and dynamic modulation of highly pure CPL could find applications for 3D displays, energy-saving organic light-emitting diode (OLED) devices, switchable lasers, and optical memory devices [65].

References

1. Maeda H, Bando Y, Shimomura K, Yamada I, Naito M, Nobusawa K, Tsumatori H, Kawai T (2011) Chemical-stimuli-controllable circularly polarized luminescence from anion-responsive π-conjugated molecules. J Am Chem Soc 133:9266–9269
2. Saleh N, Moore B, Srebro M, Vanthuyne N, Toupet L, Williams JA, Roussel C, Deol KK, Muller G, Autschbach J, Crassous J (2015) Acid/base-triggered switching of circularly polarized luminescence and electronic circular dichroism in organic and organometallic helicenes. Chem Eur J 21:1673–1681
3. Amako T, Nakabayashi K, Mori T, Inoue Y, Fujiki M, Imai Y (2014) Sign inversion of circularly polarized luminescence by geometry manipulation of four naphthalene units introduced into a tartaric acid scaffold. Chem Commun 50:12836–12839

4. Kumar J, Nakashima T, Tsumatori H, Kawai T (2014) Circularly polarized luminescence in chiral aggregates: dependence of morphology on luminescence dissymmetry. J Phys Chem Lett 5:316–321
5. Kumar J, Tsumatori H, Yuasa J, Kawai T, Nakashima T (2015) Self-discriminating termination of chiral supramolecular polymerization: tuning the length of nanofibers. Angew Chem Int Ed 54:5943–5947
6. Sethy R, Kumar J, Métivier R, Louis M, Nakatani K, Mecheri NMT, Subhakumari A, Thomas KG, Kawai T, Nakashima T (2017) Enantioselective light harvesting with perylenediimide guests on self-assembled chiral naphthalenediimide nanofibers. Angew Chem Int Ed 56:15053–15057
7. Kumar J, Kawai T, Nakashima T (2017) Circularly polarized luminescence in chiral silver nanoclusters. Chem Commun 53:1269–1272
8. Morisue M, Yumura T, Sawada R, Naito M, Kuroda Y, Chujo Y (2016) Oligoamylose-entwined porphyrin: excited-state induced-fit for chirality induction. Chem Commun 52:2481–2484
9. Yuasa J, Ueno H, Kawai T (2014) Sign reversal of a large circularly polarized luminescence signal by the twisting motion of a bidentate ligand. Chem Eur J 20:8621–8627
10. Imai Y, Nakano Y, Kawai T, Yuasa J (2018) A smart sensing method for object identification using circularly polarized luminescence from coordination-driven self-assembly. Angew Chem Int Ed 57:8973–8978
11. Nagata Y, Nishikawa T, Suginome M (2014) Chirality-switchable circularly polarized luminescence in solution based on the solvent-dependent helix inversion of poly(quinoxaline-2,3-diyl)s. Chem Commun 50:9951–9953
12. Zhang YJ, Oka T, Suzuki R, Ye JT, Iwasa Y (2014) Electrically switchable chiral light-emitting transistor. Science 344:725–728
13. Nishizawa N, Nishibayashi K, Munekata H (2017) Pure circular polarization electroluminescence at room temperature with spin-polarized light-emitting diodes. Proc Natl Acad Sci U S A 114:1783–1788
14. Sherson JF, Krauter H, Olsson RK, Julsgaard B, Hammerer K, Cirac I, Polzik ES (2006) Quantum teleportation between light and matter. Nature 443:557–560
15. Feringa BL, van Delden RA, Koumura N, Geertsema EM (2000) Chiroptical molecular switches. Chem Rev 100:1789–1816
16. Yildiz I, Deniz E, Raymo FM (2009) Fluorescence modulation with photochromic switches in nanostructured constructs. Chem Soc Rev 38:1859–1867
17. Irie M, Fukaminato T, Matsuda K, Kobatake S (2014) Photochromism of diarylethene molecules and crystals: memories, switches, and actuators. Chem Rev 114:12174–12277
18. Fukaminato T (2011) Single-molecule fluorescence photoswitching: design and synthesis of photoswitchable fluorescent molecules. J Photochem Photobiol C 12:177–208
19. Saika T, Iyoda T, Honda K, Shimidzu T (1992) Emission control of a pyrene-thioindigo compound. J Chem Soc Chem Commun 1992:591–592
20. Wang J, Kulago A, Browne WR, Feringa BL (2010) Photoswitchable intramolecular H-stacking of perylenebisimide. J Am Chem Soc 132:4191–4192
21. Heller HG, Oliver S (1981) Photochromic heterocyclic fulgides. 1. Rearrangement reactions of (E)-alpha-3-furylethylidene(isopropylidene)succinic anhydride. J Chem Soc Perkin Trans 1:197–202
22. Hayasaka H, Miyashita T, Tamura K, Akagi K (2010) Helically π-stacked conjugated polymers bearing photoresponsive and chiral moieties in side chains: reversible photoisomerization-enforced switching between emission and quenching of circularly polarized fluorescence. Adv Funct Mater 20:1243–1250
23. Berova N, Nakanishi K, Woody RW (2000) Circular dichroism: principal and applications, 2nd edn. Wiley-VCH, New York

24. Peeters M, Christiaans MPT, Janssen RAJ, Schoo HFM, Dekkers HPJM, Meijer EW (1997) Circularly polarized electroluminescence from a polymer light-emitting diode. J Am Chem Soc 119:9909–9910
25. Geng Y, Trajkovska A, Katsis D, Ou JJ, Culligan SW, Chen SH (2002) Synthesis, characterization, and optical properties of monodisperse chiral oligofluorenes. J Am Chem Soc 124:8337–8347
26. Wilson JN, Steffen W, McKenzie TG, Lieser G, Oda M, Neher D, Bunz UHF (2002) Chiroptical properties of poly(*p*-phenyleneethynylene) copolymers in thin films: large g-values. J Am Chem Soc 124:6830–6831
27. Satrijo A, Meskers SCJ, Swager TM (2006) Probing a conjugated polymer's transfer on organization-dependent properties from solutions to films. J Am Chem Soc 128:9030–9031
28. Berova N, Di Bari L, Pescitelli G (2007) Application of electronic circular dichroism in configuration and conformational analysis of organic compounds. Chem Soc Rev 36:914–931
29. Nakashima T, Atsumi K, Kawai S, Nakagawa T, Hasegawa Y, Kawai T (2007) Photochromism of thiazole-containing triangle terarylenes. Eur J Org Chem 2007:3212–3218
30. Fukumoto S, Nakashima T, Kawai T (2011) Photon-quantitative reaction of a dithiazolylarylene in solution. Angew Chem Int Ed 50:1565–1568
31. Fukumoto S, Nakashima T, Kawai T (2011) Intramolecular hydrogen bonding in a triangular dithiazolyl-azaindole for efficient photoreactivity in polar and nonpolar solvents. Eur J Org Chem 2011:5047–5053
32. Li R, Nakashima T, Galangau O, Iijima S, Kanazawa R, Kawai T (2015) Photon-quantitative 6p-electrocyclization of a diarylbenzo[*b*]thiophene in polar medium. Chem Asian J 10:1725–1730
33. Nakagawa T, Miyasaka Y, Yokoyama Y (2018) Photochromism of a spiro-functionalized diarylethene derivative: multi-colour fluorescence modulation with a photon-quantitative photocyclization reactivity. Chem Commun 54:3207–3210
34. Gavrel G, Yu P, Léaustic A, Gillot R, Métivier R, Nakatani K (2012) 4,4′-Bithiazole-based tetraarylenes: new photochromes with unique photoreactive patterns. Chem Commun 48:10111–10113
35. Nakashima T, Yamamoto K, Kimura Y, Kawai T (2013) Chiral photoresponsive tetrathiazoles that provide snapshots of folding states. Chem Eur J 19:16972–16980
36. Nakashima T, Imamura K, Yamamoto K, Kimura Y, Katao S, Hashimoto Y, Kawai T (2014) Synthesis, structure, and properties of α,β-linked oligothiazoles with controlled sequence. Chem Eur J 20:13722–13729
37. Hashimoto Y, Nakashima T, Shimizu D, Kawai T (2016) Photoswitching of an intramolecular chiral stack in a helical tetrathiazole. Chem Commun 52:5171–5174
38. Sanchez-Cárnerero EM, Agarrabeitia AR, Moreno F, Maroto BL, Muller G, Ortiz MJ, de la Moya S (2015) Circularly polarized luminescence from simple organic molecules. Chem Eur J 21:13488–13500
39. Brittain H, Ambrozich DL, Saburi M, Fendler JH (1980) Enhanced optical activity associated with chiral 1-(1-hydroxyhexyl)pyrene excimer formation. J Am Chem Soc 102:6372–6374
40. Kano K, Matsumoto H, Hashimoto S, Sisido M, Imanishi Y (1985) Chiral pyrene excimer in the γ-cyclodextrin cavity. J Am Chem Soc 107:6117–6118
41. Richardson FS, Riehl JP (1977) Circularly polarized luminescence spectroscopy. Chem Rev 77:773–792
42. Lunkley JL, Shirotani D, Yamanari K, Kaizaki S, Muller G (2008) Extraordinary circularly polarized luminescence activity exhibited by cesium tetrakis(3-heptafluoro-butylryl-(+)-camphorato) Eu(III) complexes in EtOH and $CHCl_3$ solutions. J Am Chem Soc 130:13814–13815
43. Carr R, Evans NH, Parker D (2012) Lanthanide complexes as chiral probes exploiting circularly polarized luminescence. Chem Soc Rev 41:7673–7686
44. Aspinall HC (2002) Chiral lanthanide complexes: coordination chemistry and applications. Chem Rev 102:1807–1850

45. Bing TY, Kawai T, Yuasa J (2018) Ligand-to-ligand interactions that direct formation of D_2-symmetrical alternating circular helicate. J Am Chem Soc 140:3683–3689
46. Hasegawa Y, Nakagawa T, Kawai T (2010) Recent progress of luminescent metal complexes with photochromic units. Coord Chem Rev 254:2643–2651
47. Cheng HB, Hu GF, Zhang ZH, Gao L, Gao X, Wu HC (2016) Photocontrolled reversible luminescent lanthanide molecular switch based on a diarylethene-europium dyad. Inorg Chem 55:7962–7968
48. He X, Norel L, Hervault YM, Métivier R, D'Aleo A, Maury O, Rigaut S (2016) Modulation of Eu(III) and Yb(III) luminescence using a DTE photochromic ligand. Inorg Chem 55:12635–12643
49. Hashimoto Y, Nakashima T, Yamada M, Yuasa J, Rapenne G, Kawai T (2018) Hierarchical emergence and dynamic control of chirality in a photoresponsive dinuclear complex. J Phys Chem Lett 9:2151–2157
50. Metcalf DH, Snyder SW, Demas JN, Richardson FS (1990) Chiral dynamics in the excited state of a stereochemically labile metal complex. J Phys Chem 94:7143–7153
51. Liu M, Zhang L, Wang T (2015) Supramolecular chirality in self-assembled systems. Chem Rev 115:7304–7397
52. Kumar J, Nakashima T, Kawai T (2015) Circularly polarized luminescence in chiral molecules and supramolecular assemblies. J Phys Chem Lett 6:3445–3452
53. Gopal A, Hifsudheen M, Furumi S, Takeuchi M, Ajayaghosh A (2012) Thermally assisted photonic inversion of supramolecular handedness. Angew Chem Int Ed 51:10505–10509
54. Miao W, Wang S, Liu M (2017) Reversible quadruple switching with optical, chiroptical, helicity, and macropattern in self-assembled spiropyran gels. Adv Funct Mater 27:1701368
55. Jiang H, Jiang Y, Han J, Zhang L, Liu M (2018) Helical nanostructures: chirality transfer and a photodriven transformation from superhelix to nanokebab. Angew Chem Int Ed 58:785–790
56. Hashimoto Y, Nakashima T, Kuno J, Yamada M, Kawai T (2018) Dynamic modulation of circularly polarized luminescence in photoresponsive assemblies. ChemNanoMat 4:815–820
57. Bu J, Watanabe K, Hayasaka H, Akagi K (2014) Photochemically colour-tuneable white fluorescence illuminants consisting of conjugated polymer nanospheres. Nat Commun 5:3799-1–3799-8
58. Su J, Fukaminato T, Placial JP, Onodera T, Suzuki R, Oikawa H, Brosseau A, Brisset F, Pansu R, Nakatani K, Métivier R (2015) Giant amplification of photoswitching by a few photons in fluorescent photochromic organic nanoparticles. Angew Chem Int Ed 55:3662–3666
59. Chen SH, Katsis D, Schmid AW, Mastrangelo JC, Tsutsui T, Blanton TN (1999) Circularly polarized light generated by photoexcitation of luminophores in glassy liquid-crystal films. Nature 397:506–508
60. San Jose BA, Yan J, Akagi K (2014) Dynamic switching of the circularly polarized luminescence of disubstituted polyacetylene by selective transmission through a thermotropic chiral nematic liquid crystal. Angew Chem Int Ed 53:10641–10644
61. Vicario J, Katsonis N, Ramon BS, Bastiaansen CWM, Broer DJ, Feringa BL (1999) Nanomotor rotates microscale objects. Nature 440:163
62. Hayasaka H, Miyashita T, Nakayama M, Kuwada K, Akagi K (2012) Dynamic photoswitching of helical inversion in liquid crystals containing photoresponsive axially chiral dopants. J Am Chem Soc 134:3758–3765
63. Li Y, Urbas A, Li Q (2012) Reversible light-directed red, green, and blue reflection with thermal stability enabled by a self-organized helical superstructure. J Am Chem Soc 134:9573–9576
64. Zheng ZG, Li Y, Bisoyi HK, Wang L, Bunning TJ, Li Q (2016) Three-dimensional control of the helical axis of a chiral nematic liquid crystal by light. Nature 531:352–356
65. Brandt JR, Salerno F, Fuchter MJ (2017) The added value of small-molecule chirality in technological applications. Nat Rev Chem 1:0045-1–0045-12